The Journal of Membrane Biology
https://doi.org/10.1007/s00232-020-00151-0

Towards a Quantitative Understanding of Protein–Lipid Bilayer Interactions at the Single Molecule Level: Opportunities and Challenges

Gavin M. King[1,2] · **Ioan Kosztin**[1]

Received: 14 September 2020 / Accepted: 4 November 2020

Abstract
Protein–lipid interfaces are among the most fundamental in biology. Yet applying conventional techniques to study the biophysical attributes of these systems is challenging and has left many unknowns. For example, what is the kinetic pathway and energy landscape experienced by a polypeptide chain when in close proximity to a fluid lipid bilayer? Here we review the experimental and theoretical progress we have made in addressing this question from a single molecule perspective. Some remaining impediments are also discussed.

Graphic Abstract

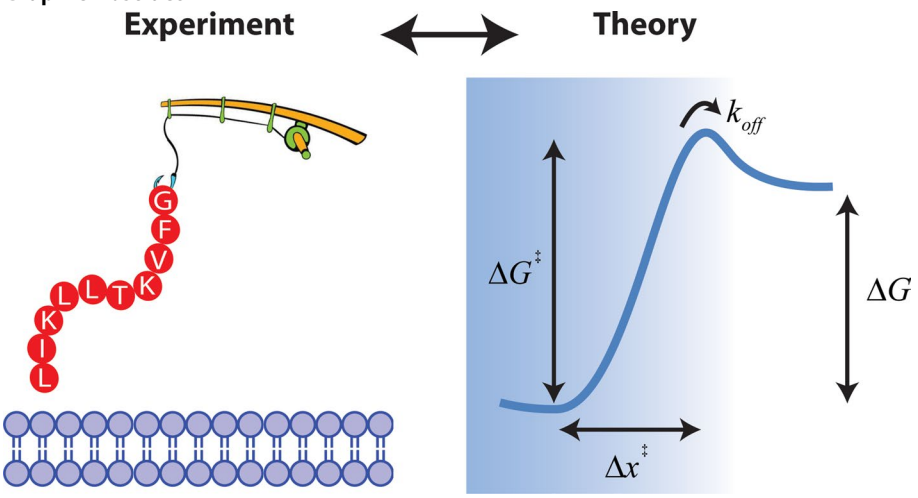

Introduction

Certain polypeptide chains freely partition into lipid bilayer membranes and form stable structures therein. Unraveling the mechanism by which this fundamental biological process occurs has fascinated researchers for decades. Indeed, a significant knowledge base has accumulated on the topic (Almeida 2014; Bowie 2005; Cymer et al. 2015; Fleming 2014; Marinko et al. 2019; Phillips et al. 2009). In seminal work in the field, Wimley and White studied a series of model peptides as they interacted with lipid bilayers (White and Wimley 1999; Wimley and White 1996). Their

✉ Gavin M. King
kinggm@missouri.edu

✉ Ioan Kosztin
kosztini@missouri.edu

[1] Department of Physics and Astronomy, University of Missouri-Columbia, Columbia, MO 65211, USA

[2] Department of Biochemistry, University of Missouri-Columbia, Columbia, MO 65211, USA

Published online: 16 November 2020

bulk equilibrium measurements employed host–guest pentapeptides of the form Trp-Leu-X-Leu-Leu with central "guest" position X representing a variable amino acid. These short protein segments spotlight the effect of peptide primary structure and allow differential comparisons of the free energy of transfer from solution to the bilayer interface, ΔG. The Wimley–White data set constitutes one of the most widely utilized hydrophobicity scales in biophysics.

Despite the importance to the field, bulk equilibrium measurements obscure the rich asynchronous dynamics that underlie polypeptide partitioning and folding in membranes. This has left significant questions unanswered including the following: What are the energy landscape and the kinetic pathway(s) underlying a peptide–lipid interaction? Further, is it possible to lift the degeneracy between certain amino acids with identical ΔG's [e.g., pentapeptides with X = Ser and X = Thr have ΔG values identical to within measurement uncertainty: 4.12 (± 0.07) and 4.11 (± 0.03) kcal/mol at pH 8, respectively (Wimley and White 1996)]? More generally, can membrane protein folding be understood at the single amino acid level? Computer simulations have shed light on some of these questions, but experimental and theoretical approaches are needed to validate such simulations (Aliste and Tieleman 2005; Chen et al. 2020; Gumbart et al. 2005; MacCallum et al. 2008; Mori et al. 2016; Pogorelov et al. 2014; Ulmschneider et al. 2011; Wang et al. 2014).

Energy landscapes (Fig. 1) provide a theoretical framework to understand how stable biomolecular structures emerge (Onuchic et al. 1997). Single molecule experimental methods are well suited for reconstructing such landscapes and have been applied to a number of systems including nucleic acids and proteins (Woodside and Block 2014). Though usually collapsed along a one-dimensional reaction coordinate and hence over-simplified, reconstructing an energy landscape can yield important insights. For example, when comparing lipophilic peptides, it may be possible to resolve differences in intrinsic off rates (k_{off}), distances to the transition state ($\Delta x^{\ddagger}$), or transition state barrier heights ($\Delta G^{\ddagger}$) that are not currently accessible. Precisely defining these quantities would not only provide a more detailed understanding of how polypeptide chains interact with lipid bilayers, but also improve predictive power.

It is important to note that the energy landscape drawn in Fig. 1, though a good starting point for discussion, depicts a simple scenario in which a peptide is either bound to the membrane in a single bound-state orientation or free in solution. A single association/dissociation pathway connects these two states in the drawing. The true situation is almost certainly more complicated. There are likely to be many intermediate states with multiple pathways interconnecting them. Additionally, membrane-induced secondary structure is common. Polypeptide chains, such as the bee-venom peptide melittin, lower the energetic cost of partitioning peptide

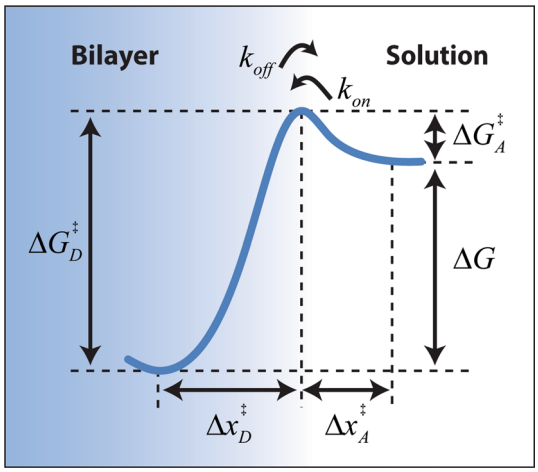

Fig. 1 Sketch of an energy landscape underling peptide–lipid interactions. A model free energy barrier (pathway) connecting the interfacial bound state and the dissociated state of a peptide is shown. Energy is plotted as a function of reaction coordinate which is taken to be distance along the membrane normal direction. Bulk equilibrium experiments yield ΔG. In principle, single molecule measurements can yield the height ($\Delta G^{\ddagger}$) and distance ($\Delta x^{\ddagger}$) to the transition state, as measured from the association, A, and dissociation, D, side of the barrier, respectively. For lipophilic peptides, it is reasonable to assume that $\Delta G_A^{\ddagger} \ll \Delta G_D^{\ddagger}$ (otherwise spontaneous partitioning of the peptide into the membrane would be a rare event) and, therefore, $\Delta G_D^{\ddagger}$ is a good (upper-bound) approximation of ΔG. Kinetic information such as the intrinsic off-rate in the absence of force, k_{off}, is also accessible via single molecule force spectroscopy

bonds by adopting amphipathic alpha-helical structure when in contact with membrane (Guha et al. 2019; Ladokhin and White 1999; White et al. 2001). An underlying stochastic driving force adds further complications (Serdiuk et al. 2016; Shibata et al. 2010). This motivates the development of a theoretical framework that can handle these complexities and describe the kinetic pathways and detailed energy landscape that quantitatively characterizes peptides in the vicinity of lipid bilayers (Utjesanovic et al. 2019).

Several experimental methods have been used to probe energy landscapes underlying protein–fluid lipid bilayer interactions at the single molecule level including optical trapping microscopes, magnetic tweezers, and atomic force microscopy (AFM) (Desmeules et al. 2002; Ma et al. 2017; Min et al. 2015; Schwierz et al. 2016). As expected, each method comes with its own advantages and drawbacks. Though extremely sensitive probes of force, optical and magnetic methods employ beads that exhibit large spatial fluctuations and are approximately two orders of magnitude larger than the apex region of an AFM tip (Fig. 2). When functionalized, the sharp needle-like geometry of an AFM tip, coupled with the translational and torsional constraints imposed by the cantilever, can limit the number of polypeptide chains available to participate in the interaction with a bilayer. An additional distinction is

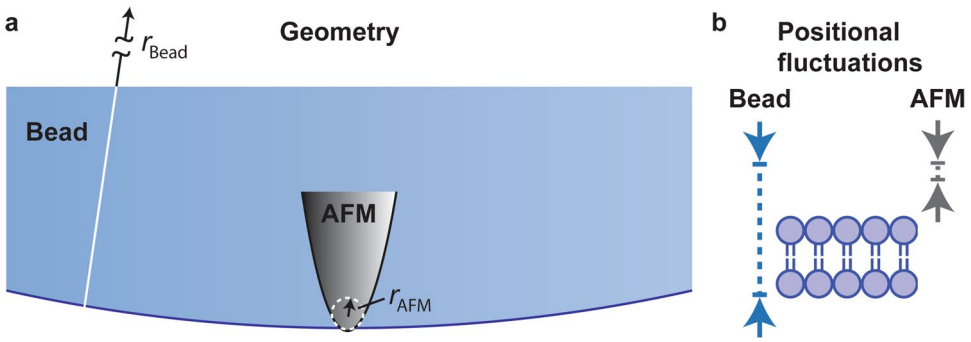

Fig. 2 Comparison between single molecule measurement techniques. **a** Cross-section of a typical bead used in an optical trapping microscope (r_{Bead} ~ 1 μm). For comparison, the apex region of a typical AFM tip (r_{AFM} ~ 10 nm) is overlaid. **b** AFM cantilevers are stiffer than optical traps, leading to lower amplitude positional fluctuations when exposed to a room temperature thermal bath, as indicated. The 4 nm thickness of the lipid bilayer serves as a natural scale bar for the comparison

that bead-based methods generally require the use of long polymer handles or linkers. Linkers commonly comprise >1000 base pair nucleic acid chains (>300 nm contour length) to which polypeptide chains are attached (Ma et al. 2017; Min et al. 2015; Perkins 2009). The added compliance of long linkers convolutes the measurement and fundamentally reduces spatial–temporal precision (Cossio et al. 2015; Walder et al. 2018). In contrast, linkers used in AFM measurements can be much shorter (<10 nm) or even non-existent. Indeed, affixing individual proteins directly to AFM tips via nonspecific interactions is typical when studying 2D crystalline arrays of membrane proteins such as bacteriorhodopsin (Oesterhelt et al. 2000; Yu et al. 2017).

Peptide–lipid interactions take place in very close proximity to and within an extremely thin membrane. Hence, when comparing instrument capabilities, a critical metric is positional noise in surface normal direction. The mechanical restoring force inherent in AFM measurements gives rise to stiffness (typical k_{AFM} ~ 10 pN/nm) that is substantially larger than that of an optically trapped bead (typical $k_{optical}$ ~ 0.1 pN/nm) (Bustamante et al. 2000). For objects in harmonic potentials such as AFM tips and optically trapped beads, increasing the stiffness, k, leads to lower positional noise as dictated by the equipartition of energy $\langle x^2 \rangle = \frac{k_B T}{k}$, where $\langle x^2 \rangle$ is the positional variance, k_B is Boltzmann's constant, and T is absolute temperature. The lower positional noise for AFM, sketched schematically by the arrows in Fig. 2b, not only reduces the requirement of signal averaging but also minimizes the potential of unintended thermally driven contact between the probe and the lipid bilayer surface. Historically, AFM has exhibited lower force precision and force stability than optical and magnetic methods, but recent advances have narrowed these gaps significantly (Churnside and Perkins 2014; Churnside et al. 2012; King et al. 2009; Walder et al. 2018). The current generation of high-precision biological AFM technology has a desirable set of attributes for probing peptide–lipid bilayer interactions at the single molecule level.

We sought to build a foundation for a more quantitative understanding of peptide–lipid interactions at the single amino acid level. Here we discuss experimental and theoretical progress our group has made along these lines (Matin et al. 2017, 2020; Utjesanovic et al. 2019). Our approach involves coupling high-precision (<1 pN) AFM-based dynamic force spectroscopy with theoretical modeling. The locus of a peripheral membrane protein–lipid bilayer interaction underling the activity of the general secretory (Sec) system of *E. coli* was used as a model system (Crane and Randall 2017). In particular, we studied the extreme N-terminus of SecA, the critical ATPase of the Sec system. Researchers have constructed a variant of SecA with the N-terminal segment deleted and replaced with a histidine tag. This SecA mutant did not support translocation in assays using standard proteoliposomes. However, when proteoliposomes were made with Ni–NTA-functionalized lipids, allowing a direct tether between the SecA mutant and the lipid bilayer surface, translocation of precursor protein was restored (Bauer et al. 2014). Hence, we focused on the extreme N-terminus of SecA, the lipophilic activity of which directly couples to protein export function in *E. coli*.

Experimental Approach

Probing protein–fluid lipid bilayer interactions at the single molecule level is a challenging endeavor that requires careful attention to the biological system as well as to the experimental technique employed. By their nature, peripheral membrane proteins bind to membranes, dissociate, and then often rebind as the cycle repeats. Such reversable association/dissociation from a membrane is amenable to study via AFM-based single molecule force spectroscopy (Fig. 3a). In contrast, integral membrane proteins do not reversibly

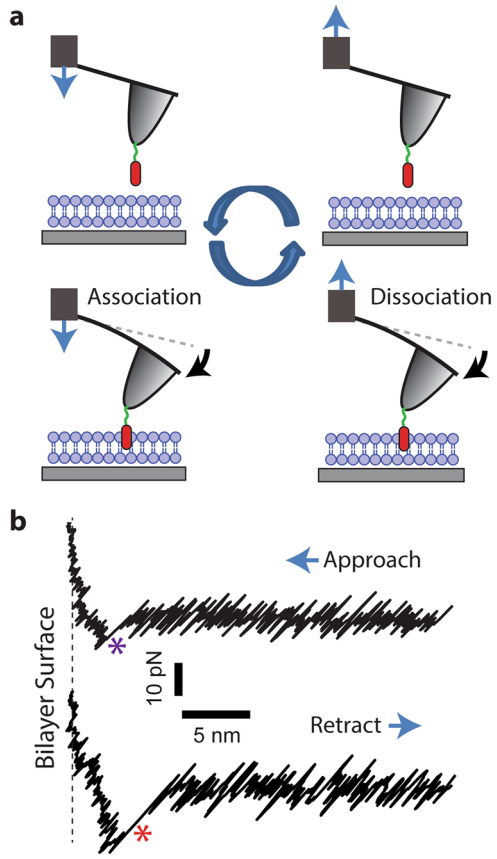

Fig. 3 Overview of AFM-based force spectroscopy experiment. **a** A functionalized AFM tip approaches and then retracts away from a supported lipid bilayer. The velocity of the base of the AFM cantilever and its equilibrium position are indicated with *blue arrows* and *dashed gray lines*, respectively. Association interactions between the peptide (*red*) and the bilayer are recorded during approach. Peptide–lipid dissociation events are observed while retracting. **b** Force spectroscopy data (force versus tip-sample separation distance) showing an individual association event (upper curve, *purple asterisk*). A dissociation event is shown in the lower curve (*red asterisk*). Such events are extracted from force versus time traces, $F(t)$, that have been converted into force versus position, $F(z)$. These data are then aggregated into histograms for further analysis. Data adapted from (Matin et al. 2017)

unbind from membrane under natural conditions, with a handful of exceptions (Kyrychenko et al. 2012; Ladokhin and Haigler 2005; Ladokhin et al. 2004; Reshetnyak et al. 2007). Forced dissociation of highly hydrophobic polypeptide chains can lead to artifacts such as pulling of lipid molecules from the membrane surface. Once dissociated from the bilayer, lipids can adhere to the functionalized tip, preventing reversibility (Andre et al. 2007).

SecA is a critical peripheral membrane protein that drives translocation of precursor proteins across the cytoplasmic membrane of *E. coli*. As the central ATPase of the Sec system, SecA is involved with nearly all steps of protein export. It forms a complex with precursor protein in the cytosol,

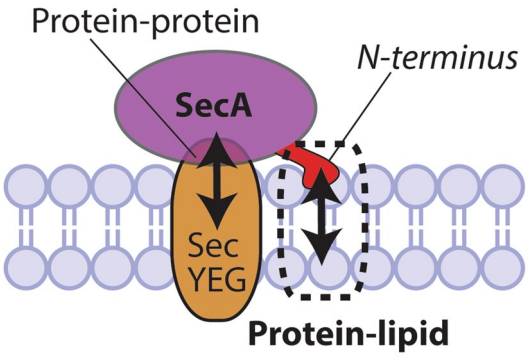

Fig. 4 SecA interactions at the membrane. We focused on the N-terminal SecA–lipid bilayer interaction which is a critical step underlying protein transport in *E. coli*

binds the cytoplasmic membrane at the translocon SecYEG, undergoes ATP binding and hydrolysis, and then dissociates back into the cytosol where the cycle can begin again (Crane and Randall 2017).

Of particular interest is the SecA–lipid bilayer interaction (Fig. 4, *dashed rectangle*). It is known that the extreme N-terminal segment of SecA binds directly to lipid, an important event underling Sec system activity (Bauer et al. 2014; Roussel and White 2020). As a starting point to understand this complex system, we studied the first 10 N-terminal amino acids of SecA (SecA2-11: `Leu-Ile-Lys-Leu-Leu-Thr-Lys-Val-Phe-Gly`) interacting with a single component zwitterionic lipid bilayer [1-palmitoyl-2-oleoyl-glycero-3-phosphocholine (POPC)] using precision AFM-based dynamic force microscopy (Churnside et al. 2012; Matin et al. 2017, 2020; Utjesanovic et al. 2019). Peptides were synthesized with a C-terminal cysteine, enabling site-specific covalent linkage to the AFM tip through a ~9.5-nm-long flexible hydrophilic linker [24 ethylene oxide (PEG) subunits] (Zimmermann et al. 2010). This short linker minimizes interactions with the surface of the AFM tip while allowing multiple binding orientations in the bilayer. Supported lipid bilayers were formed via vesicle fusion on clean glass surfaces, mimicking the cellular membrane (Sackmann 1996). Figure 3b shows representative peptide–lipid interaction traces.

Several experiments are warranted to bolster confidence in the experimental approach and in its quantitative interpretation. First, to evaluate specificity of the interactions, we mimicked the final experimental design, but with peptide omitted. Specifically, we examined tips functionalized with NHS-PEG-maleimide-`Cys` as they interacted with glass-supported POPC lipid bilayers. This produced 13 dissociation events (>5 pN) out of 500 attempts with 5 distinct tips (Fig. 5a) (Matin et al. 2017). No association interactions (>5 pN) were observed (*data not shown*). The results indicate that all association events arise from specific

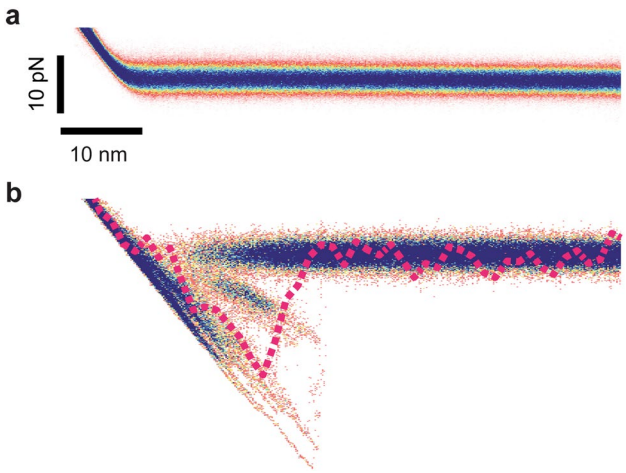

Fig. 5 Control experiments verify interaction specificity and evaluate lipid adhesion to the peptide-functionalized tip. **a** Density plot showing superimposed force versus distance retraction data for tips lacking the SecA2-11 peptide ($N = 500$ curves from $N_t = 5$ distinct tips). **b** The very first retraction interaction (*dotted pink line*) between a new, freshly functionalized SecA2-11 tip and a supported POPC bilayer. This force-distance curve is overlaid on a density plot of all subsequent curves recorded with the same identical tip ($N = 100$). Data were acquired with a pulling speed of 100 nm/s, adapted from (Matin et al. 2017)

peptide–lipid interactions and there is a low propensity (<3 %) for non-specific dissociation events (Matin et al. 2017). Next, we tested for lipid adhesion to the tip upon peptide dissociation from the bilayer, as has been reported in other systems (Andre et al. 2007). To evaluate this, we compared the very first force curve acquired with a freshly functionalized SecA2-11 tip with subsequent force curves using the same identical tip (Fig. 5b). Based on the good overall agreement between the first force versus distance curve and all of the subsequent curves, lipid adhesion to the tip for this peptide–lipid system can be ruled out.

We also carried out experiments to verify that specific changes in peptide geometry alter the force spectra in predictable ways. In addition to the core SecA2-11 sequence, peptide constructs with nearly identical chemical composition, but with differing geometry were synthesized: two copies of SecA2-11 linked in series, and two copies in parallel. The data indicate (Fig. 6) that lipid bilayer partitioning interactions of peptides with differing geometry can be distinguished. The 2D density plots show height versus dissociation force (Fig. 6, *top row*) or association force (Fig. 6, *bottom row*) with supported POPC bilayers. We note that height is defined as the position of the tip apex above the bilayer when the dissociation or association event occurred. Both of the dimeric constructs (i.e., series and parallel) exhibited a population of dissociation events at approximately the same location in position-force space (~4 nm, ~18 pN) as the single copy peptide (Fig. 6, *Top row*). This was the only prominent population observed for the monomeric construct. In contrast, the dimeric series construct exhibited a bimodal position-space distribution with a second and more pronounced population centered at similar force, but at a higher position above the bilayer. MD simulations suggested that the population of events at the lower position (~3.8 nm) is likely due to a compact conformation of the series peptide (Matin et al. 2017). The parallel construct, in contrast to both single copy and series, exhibited a long tail of dissociation events extending well beyond 50 pN. This tail contained a significant fraction of the total population (40%) and appeared likely to be associated with pulling of lipid molecules from the bilayer surface (Stetter et al. 2014; Wieland et al. 2005). Indeed, control experiments with lipid bilayers comprising the same PC head groups, but rigidified with photo-polymerized tail groups, provided evidence that this was likely occurring with the parallel dimer construct (Fig. 7).

One may intuitively expect that higher dissociation forces would be required for the dimeric peptide constructs because the number of hydrophobic residues is twice of that of the monomer. However, the interaction of the dimeric constructs was not additive with respect to the monomer, consistent with other work (Ladokhin and White 2001). Rather, the data indicated that intra-peptide interactions occurring within the dimeric series construct were competing with the bilayer. This resulted in the parallel dimer being significantly more lipid-active than the series. In particular, an approximate fivefold greater probability of bilayer association, A, was observed for the parallel construct compared to the series (Fig. 6, *Bottom row*). To summarize, prominent signatures in the force spectra mapped to specific peptide geometries. These results engender confidence in the overall experimental approach.

Recently, we extended the methodology to bilayers comprising *E. coli* polar lipid and probed the locus of this critical SecA–lipid interaction in near-native conditions. Repeated mechanical dissociation of (single copy) SecA2-11 from supported *E. coli* polar lipid bilayers generated dissociation force histograms, also known as rupture force distributions, $P(\mathrm{F})$. An example $P(\mathrm{F})$ for 50 nm/s pulling speed is shown (Fig. 8a). Theoretical modeling revealed several interesting features in a complex energy landscape. By modeling the dissociation process as a diffusive escape over an energy barrier, the dissociation force data were connected to kinetic parameters. Four dissociation pathways were needed to model the experimental data, two "single" pathways and two "double" pathways (see "Theoretical Approach" section for details). To constrain the fits, energy landscape parameters $\Delta G^{\ddagger}$ and $\Delta x^{\ddagger}$ were estimated from molecular dynamics simulations and held fixed, but this is not a hard requirement. Alternatively, $\Delta G^{\ddagger}$ and $\Delta x^{\ddagger}$ can be used as fitting parameters (Matin et al. 2017). Catch bond behavior was evident at

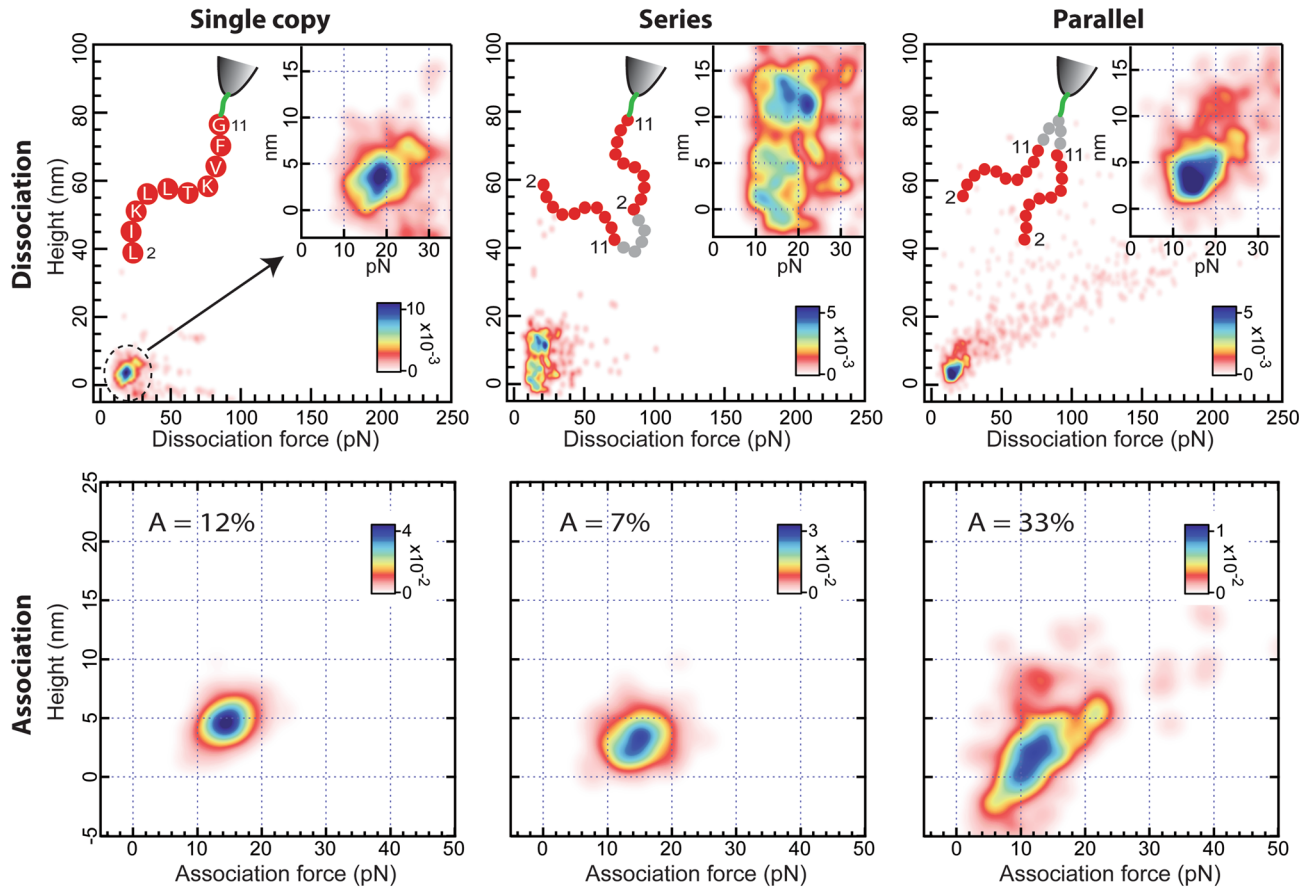

Fig. 6 Force spectroscopy data correlates with peptide geometry. (Top row) Two-dimensional probability density plots of dissociation height versus force for single copy SecA2-11 and POPC ($N=303$, $N_t=5$). Dissociation data for the series ($N=357$, $N_t=5$) and parallel ($N=667$, $N_t=8$) peptide constructs are also shown. Cartoon insets show glycine-rich linkers (*gray*) connecting the two copies of SecA2-11 (*red*) for the dimeric constructs. (Bottom row) Probability distributions showing association events for the three peptide constructs: single copy ($N=261$, $N_t=8$), series ($N=205$, $N_t=9$), and parallel ($N=217$, $N_t=8$). Association probabilities, A, are also indicated for each peptide. Data were acquired with an advancing/retraction speed of 100 nm/s, adapted from (Matin et al. 2017)

certain pulling speeds (Fig. 8b, *arrows*). Usually increasing force loading on an intermolecular bond makes the bond rupture faster. However, the opposite occurs with a catch bond (Marshall et al. 2003). In this case, the lifetime of the bond increases with increasing force loading.

Electrostatic effects have a significant influence on peptide–lipid bilayer interactions (Fernandez-Vidal et al. 2011; Ladokhin and White 2001; Posokhov et al. 2007; Vasquez-Montes et al. 2018). In our experiments with anionic membrane, structural sturdiness accompanying secondary structure was evident. Circular dichroism measurements indicated that SecA2-11 adopted little helical structure when bound to zwitterionic PC head groups, but secondary structure, which rigidifies the lipid-bound polypeptide, emerged when negatively charged 1-palmitoyl-2-oleoyl-sn-glycero-3-phospho-(1′-rac-glycerol) (PG) lipid was present in the bilayer (Matin et al. 2020). Rupture force distributions indicated an approximate twofold enhancement of double-rupture pathways for *E. coli* polar lipid over zwitterionic PC. We hypothesized that because an alpha-helical peptide is more mechanically stiff (exhibits a significantly larger persistence length and Young's modulus), it is more likely to simultaneously dissociate multiple residues compared to an unstructured peptide when subject to the same force loading conditions. Further, the structural rigidity of the *E. coli* polar lipid-bound SecA2-11 may play an important role in propagating conformational changes to distal regions of SecA, influencing translocation activity.

Despite complexities including multiple dissociation pathways, secondary structure formation, and catch bonding, a well-defined lipid bilayer dissociation rate in the absence of force was obtained over multiple pulling speeds of the AFM cantilever (Fig. 8b, *inset*). Specifically, we determined the *E. coli* polar lipid bilayer-bound-state lifetime of SecA2-11 in the absence of force to be $\tau_o^{\text{lipid}} = \frac{1}{k_{\text{off}}} = 1.18$ s. This is

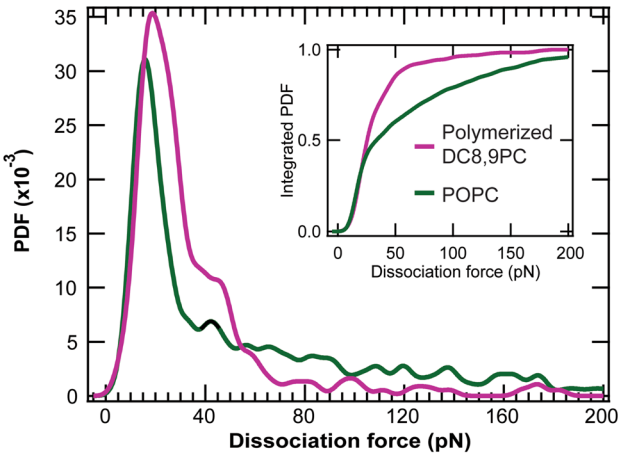

Fig. 7 Pulling of lipid molecules off the surface assayed via photo-polymerized bilayer. Distribution of dissociation events for the parallel SecA2-11 construct using photo-polymerized1,2-bis(10,12-tricosadiynoyl)-sn-glycero-3-phosphocholine (DC8,9PC) lipid bilayers (*purple*; $N=701$, $N_t=8$). For reference, data using standard POPC are overlaid (*green*; $N=667$, $N_t=8$). Inset: integrated probability densities. Data adapted from (Matin et al. 2017)

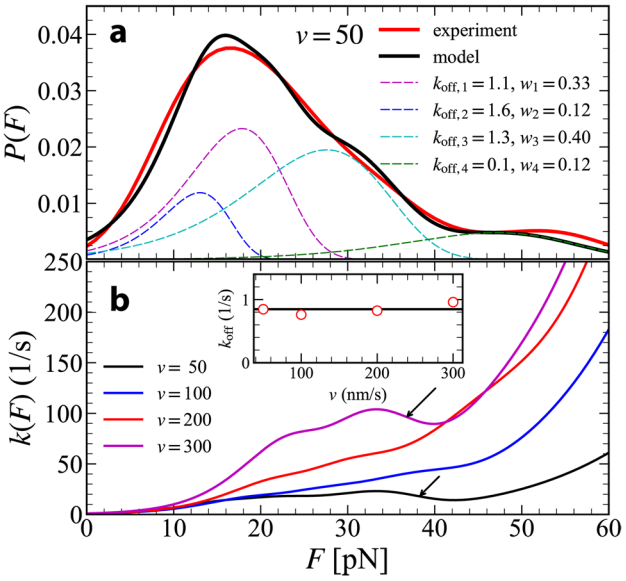

Fig. 8 SecA2-11 dissociation from *E. coli* polar lipid bilayers and kinetics analysis. **a** Dissociation force distribution, $P(F)$, for SecA2-11 and *E. coli* polar lipid. Four dissociation pathways (labeled 1–4) are required to fit the theoretical model (*solid black curve*) to the experimental result (*solid red curve*). The first two pathways are *single* dissociations, with $\Delta G_1^{\ddagger} = 8kT$, $\Delta x_1^{\ddagger} = 1$ nm, and $\Delta G_2^{\ddagger} = 10kT$, $\Delta x_2^{\ddagger} = 1.3$ nm, respectively. The last two pathways correspond to *double* dissociations with the same activation energy and length as the second pathway. Contributions to $P(F)$ from the individual pathways are shown as colored dashed curves; the corresponding off rates ($k_{\text{off},i}$) and weights (w_i) are listed. Data acquired with the base of the AFM cantilever retracting at a speed of $v = 50$ nm/s, adapted from (Matin et al. 2020). **b** Force-dependent dissociation rate, $k(F)$, for SecA2-11 and *E. coli* polar lipid, for four retraction speeds (listed in nm/s). Two *catch bond* regions [where the slope of $k(F)$ is < 0] are marked with arrows. Inset: Retraction speed dependence of the intrinsic off-rate, $k_{\text{off}} = k(0)$. The horizontal line represents the mean value $\langle k_{\text{off}} \rangle = 0.85\text{s}^{-1}$

significantly larger than the fundamental timescale of the secretion process (~50 ms), suggesting that lipid interactions alone play a significant role in stabilizing SecA on the bilayer during translocation. We note that τ_o^{lipid} is slightly larger than the previously reported value [$\tau_o^{\text{lipid}} = 0.9$ s (Matin et al. 2020)] due to differences in the fitting algorithm employed.

Theoretical Approach

Similar to other force-induced molecular transitions [e.g., unfolding of protein (Cecconi et al. 2005; Kellermayer et al. 1997; Marszalek et al. 1999; Rief et al. 1997; Schlierf et al. 2004; Schlierf and Rief 2006), unzipping of nucleic acids (Greenleaf et al. 2008; Liphardt et al. 2001), ligand-receptor dissociation (Florin et al. 1994; Merkel et al. 1999)], the forced dissociation of peripheral membrane proteins or their constitutive polypeptide chains from lipid bilayers can be modeled as a stochastic Brownian escape process across a free energy barrier (Bell 1978; Dudko et al. 2006; Evans and Ritchie 1997; Hummer and Szabo 2003), whose size and shape are modulated by applied force. In general, such a dissociation pathway is characterized by three model parameters, namely, (1) the barrier height or *activation energy*, $\Delta G^{\ddagger}$; (2) the separation distance (normal to the plane of the membrane) between the bound and transition states or *activation length*, $\Delta x^{\ddagger}$; and (3) the intrinsic dissociation (off-) rate, k_{off}.

A seminal contribution from Stephen White's laboratory is the identification of the interfacial zone of lipid bilayer structure (Wiener and White 1992). As a result, the energetics of protein–lipid interactions should be analyzed in the context of (1) *interfacial* and (2) *transmembrane* zones. Our analyses focused on the last rupture events recorded in the force versus time traces (i.e., immediately before the peptide dissociated from the bilayer and entered the solution above). Due to the geometry of the force spectroscopy experiments, this last rupture event likely emanates from the interfacial bilayer zone.

When an external pulling force, F, is applied to the peptide to facilitate its dissociation from the membrane, both $\Delta G^{\ddagger}$ and $\Delta x^{\ddagger}$ decrease, resulting in an enhanced force-dependent dissociation rate, $k(F)$. It is important to note that $k(F)$ is model dependent and is a monotonically increasing function of F for an individual dissociation pathway (Utjesanovic et al. 2019). The values of all the parameters are determined by fitting the theoretical model to the experimental results. However, it is not $k(F)$ that is measured in

experiments, but rather the dissociation force distribution, $P(F)$, which is the histogram of rupture forces recorded in repeated AFM retraction experiments. Fortunately, for a given force loading rate $\dot{F}$ (which, in force-ramp experiments, is a known constant), there exists simple, model-independent equations that connect $k(F)$ to $P(F)$ and vice versa. Because $k(F)$ is more sensitive to the variation of the force (especially at large F) than $P(F)$, it is usually easier to determine the values of the model parameters by fitting the latter instead of the former.

There are at least two features that set peptide–lipid membrane dissociation apart from other force-induced molecular transitions (Matin et al. 2017, 2020; Utjesanovic et al. 2019). First, the value of the activation energy is relatively small, i.e., $\Delta G^{\ddagger} \leq 10kT$, especially for polypeptide chains stemming from the membrane interaction loci of peripheral membrane proteins that bind predominantly at the interfacial zone of the bilayer. Thus, the direct application of any of the two most popular models for determining $k(F)$, i.e., the Bell–Evans (BE) model (Bell 1978; Evans and Ritchie 1997) and the Dudko–Hummer–Szabo (DHS) model (Dudko et al. 2006, 2008), are questionable because they both rely on Kramers theory of barrier crossing (Kramers 1940), which is valid only for large barriers. In order to address this shortcoming, we have extended the DHS model for barriers of arbitrary size by defining $k(F)$ as the inverse mean first passage time (MFPT) across the barrier (Utjesanovic et al. 2019). Figure 9 compares the force dependence of $k(F)$ and $P(F)$ from our MFPT model with those from the BE and DHS models for force and pathway parameter values typical to peptide–lipid membrane dissociation. While clearly BE is not suitable for a quantitative description of peptide–membrane interactions, the difference between the DHS and MFPT models is significant only at the higher end of the force range. Indeed, $k(F)$ from DHS (Fig. 9a), after the expected increase with F, reaches a maximum value after which it decreases and eventually vanishes at a critical force $F_c = \alpha(\Delta G^{\ddagger}/\Delta x^{\ddagger})$, where α is a numerical constant (of order unity) specific to the shape of the dissociation-free energy profile. This unphysical behavior, which signals the breakdown of the DHS model for low barriers (i.e., for $\Delta G^{\ddagger} \sim F\Delta x^{\ddagger}$), is removed in our MFPT model, where $k(F)$, as expected, increases monotonically with F until it diverges at F_c, where the barrier vanishes. It should be noted, however, that in spite of this difference, the dissociation force distributions calculated with the DHS and MFPT models give almost the same result (Fig. 9c), simply because the contribution of the large F region to $P(F)$ is exponentially small. Furthermore, as shown (Fig. 9b, d), at sufficiently high barriers (i.e., $\Delta G^{\ddagger} \geq 15kT$) both the DHS and MFPT models give essentially the same results for $k(F)$ and $P(F)$ over the relevant force range and their differences with respect to the high barrier BE results are manifestly reduced.

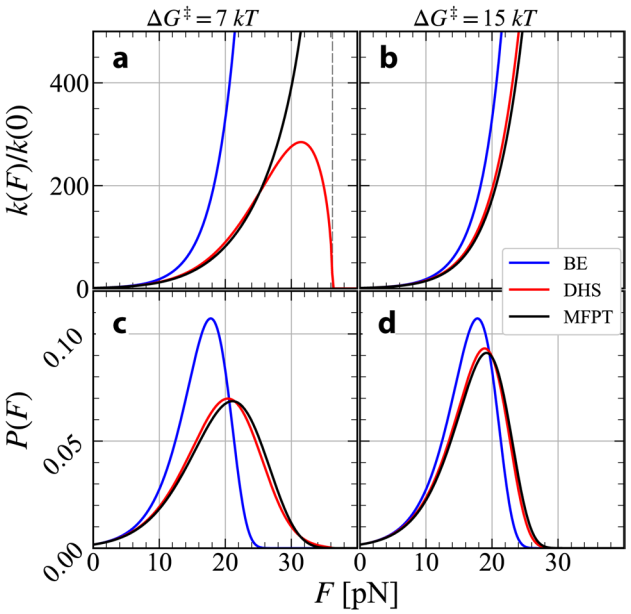

Fig. 9 Effect of free energy barrier height on theoretical models. **a**, **b** Comparison between the force-dependent dissociation rate $k(F)$ for a single pathway from theoretical models BE (*blue lines*), DHS (*red lines*), and MFPT (*black lines*) subject to two different barrier heights. **c**, **d** Similar comparison for the dissociation force distribution $P(F)$. Panels **a** and **c** (**b** and **d**) correspond to a low (high) barrier of $\Delta G^{\ddagger} = 7kT$ ($\Delta G^{\ddagger} = 15kT$). The values used for all the other model parameters were held fixed: $\Delta x^{\ddagger} = 1.2$ nm, $k_{off} = 0.5s^{-1}$, and loading rate $\dot{F} = 300$ pN/s

A second distinctive feature of peptide–lipid dissociation is the (usually) broad, multimodal structure of the experimentally measured $P(F)$, which indicates that more than one dissociation pathways are in play (Matin et al. 2017, 2020; Utjesanovic et al. 2019). A simple method to verify the validity of the multiple dissociation pathways hypothesis is to calculate and plot the corresponding $k(F)$. Indeed, in the case of stochastic mixing of two or more pathways, $k(F)$ will be *nonmonotonic* and, for some intermediate force regions, will exhibit catch bond behavior where, contrary to expectations, the forced dissociation rate decreases while the force is increased (i.e., $dk/dF < 0$). The presence of multiple dissociation pathways in peptide–lipid membrane interactions is most likely due to the complexity of the system. Because the experimentally measured $P(F)$ represents a stochastic mixing of multiple pathways, it should not come as a surprise that the results may differ significantly for experiments set up and performed under the exact same conditions (Utjesanovic et al. 2019). In such cases the theoretical modeling also becomes more involved. Indeed, assuming $i = 1, \ldots, N$ dissociation pathways, each characterized by a triplet of values $(\Delta G_i^{\ddagger}, \Delta x_i^{\ddagger}, k_{\mathrm{off},i})$, the measured force distribution must be fit to $P(F) = \sum_{i=1}^{N} w_i P_i(F)$, where the weight

coefficients w_i of each pathway should also be regarded as fitting parameters (Utjesanovic et al. 2019).

Another possible complication relevant to peptide–lipid membrane dissociation is due to the existence of the so-called "double" rupture events (Matin et al. 2020; Utjesanovic et al. 2019). An example of such an event is when the tip of the cantilever contains more than one peptide and two of these dissociate from the bilayer in such rapid succession such that the AFM cannot resolve them in time. If the dissociation of a small peptide from a membrane can occur only along a single pathway, the finite probability of "double" ruptures (besides the regular "single" ruptures) can render the rupture force distribution effectively bimodal. The situation is illustrated in Fig. 10 for the same model parameters as those in Fig. 9 and assuming that $w_1 = 0.6$ ($w_2 = 0.4$) for "single" ("double") ruptures. We find again that the BE model is not suitable for describing peptide–lipid membrane dissociation, while DHS and our MFPT model give essentially the same result apart from $k(F)$ at the largest forces considered. Because the "double" ruptures constitute a separate pathway, as expected, $k(F)$ has a narrow catch bond region (with $dk/kF < 0$) at intermediate forces.

In general, a small number of pathways including both "single" and "double" ruptures, characterized by well-defined parameter values ($\Delta G_i^{\ddagger}$, $\Delta x_i^{\ddagger}$, $k_{\mathrm{off},i}$), are sufficient to model the experimentally measured dissociation force distribution $P(F)$ of the peptide–lipid membrane system. However, the model can be further improved by regarding the pathway parameters themselves as stochastic variables and characterizing their distribution by employing Bayesian inference methods.

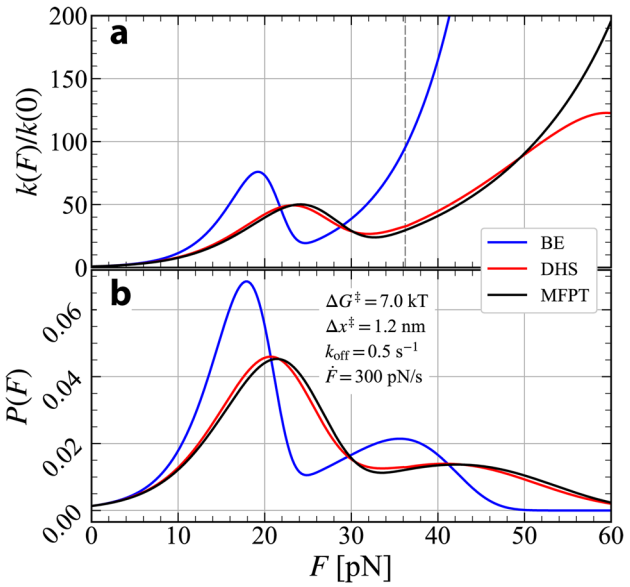

Fig. 10 Stochastic mixing of single- and double-rupture events. Comparison between the **a** force-dependent dissociation rate $k(F)$ for a stochastic mixture of 60% "single" and 40% "double" ruptures involving a dissociation pathway (parameters listed in panel B) and **b** dissociation force distribution $P(F)$, generated from the BE (*blue lines*), DHS (*red lines*), and MFPT (*black lines*) models, described in the text

Conclusions and Outlook

We reviewed our recent work on peptide–fluid lipid bilayer interactions via single molecule AFM-based dynamic force spectroscopy. The study focused on the locus of a peripheral membrane protein interaction essential for protein export activity in *E. coli*. Surprisingly, the relatively short 10-amino-acid-long SecA2-11 peptide–*E. coli* polar lipid interaction exhibited rich kinetic behavior. Control experiments bolstered confidence in the experimental data. Comparisons between molecular dynamics simulations and recent electron paramagnetic resonance measurements provide further corroboration of the approach (Findik et al. 2018; Matin et al. 2020). Theoretical analysis of SecA2-11 interactions with lipid bilayers revealed a complex energy landscape complete with multiple dissociation pathways as well as catch bond behavior. In the face of this complexity, a well-defined lipid bilayer dissociation rate in the absence of force was obtained. The value determined with *E. coli* polar lipid ($\tau_{\mathrm{o}}^{\mathrm{lipid}} \sim 1.2$ s) is well separated from and is significantly larger than the fundamental timescale of the protein secretion process (~0.05 s), defined as the time for a single amino acid to be translocated through the translocon (Kramer et al. 2009). Thus, lipid interactions alone appear capable of stabilizing SecA on the bilayer for a time period commensurate with the translocation of >10 amino acids. However, the measurements do not account for stabilization that likely occurs in full-length SecA through direct contacts with the translocon SecYEG or with precursors. We expect the $\tau_{\mathrm{o}}^{\mathrm{lipid}}$ result to represent a lower limit for in vivo conditions. Characterizing the SecA2-11–*E. coli* lipid interaction represents a step towards a more quantitative understanding of the interplay between SecA, the membrane surface, and SecYEG during the translocation process.

Can single molecule force spectroscopy of protein–fluid lipid bilayers be extended further towards native biological systems? There are a number of longer polypeptide chains found in nature that may be amenable to the method. These include the bee-venom peptide melittin and other membrane-active peptides which form amphipathic helices on the bilayer surface (Guha et al. 2019). For the Sec system, a logical step in this direction would be to employ full-length SecA with an appropriately positioned handle distal to the N-terminal region (Fig. 11a). Several interesting and longstanding questions could be addressed with this assay. For example, does the SecA–lipid bilayer interaction strength vary with the ATP hydrolysis state of this enzyme? Does the presence of precursor proteins bound to SecA

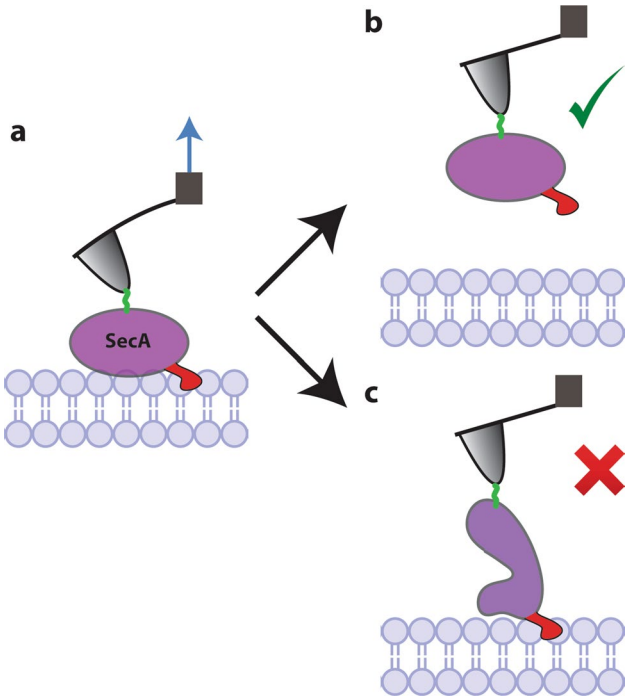

Fig. 11 A possible future direction. **a** Extending AFM-based single molecule force spectroscopy methodology to probe full-length SecA–*E. coli* lipid bilayer interactions. **b** Ideally, dissociation would lead to release of SecA from the membrane without denaturing. **c** However, destabilizing the structure (e.g., breaking tertiary interactions) is possible during this process

affect the interaction? Further, if the liposomes were to be reconstituted with active translocons SecYEG (Mao et al. 2013; Sanganna Gari et al. 2019), one could explore how contacts between the membrane external cytoplasmic loops of SecYEG modulate the SecA–membrane interaction. If the tertiary contacts stabilizing SecA structure are stronger than the protein–membrane interaction (Fig. 11b), then the approach should bear fruit. Alternatively, SecA could partially or fully unfold (Fig. 11c). Despite this potentiality, detecting this non-native artifact would be straight forward—the last rupture event would occur well above the surface of the bilayer. If observed, SecA may be allowed to refold, alleviating the need of changing tips.

Probing polypeptide chains from integral membrane proteins such as full transmembrane helices remains challenging to study with fluid lipid bilayers. A potential path forward would be to focus on the handful of systems and conditions that have exhibited reversibility (Kyrychenko et al. 2012; Ladokhin and Haigler 2005; Ladokhin et al. 2004; Reshetnyak et al. 2007). Additionally, rigidifying the bilayer by crosslinking lipid tails (Matin et al. 2017) or employing lipid nanodiscs (Zocher et al. 2012) may limit pulling of lipid molecules and allow the method to generalize, but these methods come with their own complications and are a step away from native biological conditions. In addition to experimental hurdles, there are theoretical obstacles. The retraction force time series, $F(t)$, contains detailed information about the entire polypeptide chain-lipid bilayer dissociation process. For highly hydrophobic chains, such as a transmembrane helix, this will likely include intermediate rupture events which are attributable to the transmembrane zone in addition to dissociation event(s) originating at the interfacial zone. To analyze the free energy profile that extends to the hydrophobic bilayer core would require a comprehensive study of the full time series, including intermediate rupture events. Further work is needed to apply and test the theory for such experiments.

Acknowledgements The research described herein was largely inspired by Steven H. White's work and by many valuable and lively discussions with him and his former group members including especially Martin B. Ulmscheinder, Kalina Hristrova, William C. Wimley, and Alexey Ladokhin. We also gratefully acknowledge discussions with Linda L. Randall, Krishna P. Sigdel, Tina R. Matin, and Milica Utjesanovic. This work was supported by the National Science Foundation (Award #: 1054832 and 1709792, G.M.K.) and the University of Missouri Research Board. The computation for this work was performed on the HPC infrastructure provided by RCSS and supported in part by the NSF under grant number CNS-1429294 at the University of Missouri-Columbia.

References

Aliste MP, Tieleman DP (2005) Computer simulation of partitioning of ten pentapeptides Ace-WLXLL at the cyclohexane/water and phospholipid/water interfaces. BMC Biochem 6:30

Almeida PF (2014) Membrane-active peptides: binding, translocation, and flux in lipid vesicles. Biochim Biophys Acta 1838:2216–2227

Andre G, Brasseur R, Dufrene YF (2007) Probing the interaction forces between hydrophobic peptides and supported lipid bilayers using AFM. J Mol Recogn JMR 20:538–545

Bauer BW, Shemesh T, Chen Y, Rapoport TA (2014) A "push and slide" mechanism allows sequence-insensitive translocation of secretory proteins by the SecA ATPase. Cell 157:1416–1429

Bell GI (1978) Models for the specific adhesion of cells to cells. Science (New York, N Y) 200:618–627

Bowie JU (2005) Solving the membrane protein folding problem. Nature 438:581–589

Bustamante C, Macosko JC, Wuite GJ (2000) Grabbing the cat by the tail: manipulating molecules one by one. Nat Rev Mol Cell Biol 1:130–136

Cecconi C, Shank EA, Bustamante C, Marqusee S (2005) Direct observation of the three-state folding of a single protein molecule. Science 309:2057–2060

Chen CH, Melo MC, Berglund N, Khan A, de la Fuente-Nunez C, Ulmschneider JP, Ulmschneider MB (2020) Understanding and modelling the interactions of peptides with membranes: from partitioning to self-assembly. Curr Opin Struct Biol 61:160–166

Churnside AB, Perkins TT (2014) Ultrastable atomic force microscopy: improved force and positional stability. FEBS Lett 588:3621–3630

Churnside AB, Sullan RM, Nguyen DM, Case SO, Bull MS, King GM, Perkins TT (2012) Routine and timely sub-picoNewton force stability and precision for biological applications of atomic force microscopy. Nano Lett 12:3557–3561

Cossio P, Hummer G, Szabo A (2015) On artifacts in single-molecule force spectroscopy. Proc Natl Acad Sci USA 112:14248–14253

Crane JM, Randall LL (2017) The sec system: protein export in *Escherichia coli*. EcoSal Plus 7

Cymer F, von Heijne G, White SH (2015) Mechanisms of integral membrane protein insertion and folding. J Mol Biol 427:999–1022

Desmeules P, Grandbois M, Bondarenko VA, Yamazaki A, Salesse C (2002) Measurement of membrane binding between recoverin, a calcium-myristoyl switch protein, and lipid bilayers by AFM-based force spectroscopy. Biophys J 82:3343–3350

Dudko OK, Hummer G, Szabo A (2006) Intrinsic rates and activation free energies from single-molecule pulling experiments. Phys Rev Lett 96:108101

Dudko OK, Hummer G, Szabo A (2008) Theory, analysis, and interpretation of single-molecule force spectroscopy experiments. P Natl Acad Sci USA 105:15755–15760

Evans E, Ritchie K (1997) Dynamic strength of molecular adhesion bonds. Biophys J 72:1541–1555

Fernandez-Vidal M, White SH, Ladokhin AS (2011) Membrane partitioning: "classical" and "nonclassical" hydrophobic effects. J Membr Biol 239:5–14

Findik BT, Smith VF, Randall LL (2018) Penetration into membrane of amino-terminal region of SecA when associated with SecYEG in active complexes. Protein Sci 27:681–691

Fleming KG (2014) Energetics of membrane protein folding. Annu Rev Biophys 43:233–255

Florin EL, Moy VT, Gaub HE (1994) Adhesion forces between individual ligand-receptor pairs. Science 264:415–417

Greenleaf WJ, Frieda KL, Foster DA, Woodside MT, Block SM (2008) Direct observation of hierarchical folding in single riboswitch aptamers. Science 319:630–633

Guha S, Ghimire J, Wu E, Wimley WC (2019) Mechanistic landscape of membrane-permeabilizing peptides. Chem Rev 119:6040–6085

Gumbart J, Wang Y, Aksimentiev A, Tajkhorshid E, Schulten K (2005) Molecular dynamics simulations of proteins in lipid bilayers. Curr Opin Struct Biol 15:423–431

Hummer G, Szabo A (2003) Kinetics from nonequilibrium single-molecule pulling experiments. Biophys J 85:5–15

Kellermayer MS, Smith SB, Granzier HL, Bustamante C (1997) Folding-unfolding transitions in single titin molecules characterized with laser tweezers. Science 276:1112–1116

King GM, Carter AR, Churnside AB, Eberle LS, Perkins TT (2009) Ultrastable atomic force microscopy: atomic-scale stability and registration in ambient conditions. Nano Lett 9:1451–1456

Kramer G, Boehringer D, Ban N, Bukau B (2009) The ribosome as a platform for co-translational processing, folding and targeting of newly synthesized proteins. Nat Struct Mol Biol 16:589–597

Kramers HA (1940) Brownian motion in a field of force and the diffusion model of chemical reactions. Physica 7:284–304

Kyrychenko A, Rodnin MV, Posokhov YO, Holt A, Pucci B, Killian JA, Ladokhin AS (2012) Thermodynamic measurements of bilayer insertion of a single transmembrane helix chaperoned by fluorinated surfactants. J Mol Biol 416:328–334

Ladokhin AS, Haigler HT (2005) Reversible transition between the surface trimer and membrane-inserted monomer of annexin 12. Biochemistry Us 44:3402–3409

Ladokhin AS, Legmann R, Collier RJ, White SH (2004) Reversible refolding of the diphtheria toxin T-domain on lipid membranes. Biochemistry Us 43:7451–7458

Ladokhin AS, White SH (1999) Folding of amphipathic alpha-helices on membranes: energetics of helix formation by melittin. J Mol Biol 285:1363–1369

Ladokhin AS, White SH (2001) Protein chemistry at membrane interfaces: non-additivity of electrostatic and hydrophobic interactions. J Mol Biol 309:543–552

Liphardt J, Onoa B, Smith SB, Tinoco I Jr, Bustamante C (2001) Reversible unfolding of single RNA molecules by mechanical force. Science 292:733–737

Ma L, Cai Y, Li Y, Jiao J, Wu Z, O'Shaughnessy B, De Camilli P, Karatekin E, Zhang Y (2017) Single-molecule force spectroscopy of protein–membrane interactions. Elife 6

MacCallum JL, Bennett WF, Tieleman DP (2008) Distribution of amino acids in a lipid bilayer from computer simulations. Biophys J 94:3393–3404

Mao C, Cheadle CE, Hardy SJ, Lilly AA, Suo Y, Sanganna Gari RR, King GM, Randall LL (2013) Stoichiometry of SecYEG in the active translocase of *Escherichia coli* varies with precursor species. Proc Natl Acad Sci USA 110:11815–11820

Marinko JT, Huang H, Penn WD, Capra JA, Schlebach JP, Sanders CR (2019) Folding and misfolding of human membrane proteins in health and disease: from single molecules to cellular proteostasis. Chem Rev 119:5537–5606

Marshall BT, Long M, Piper JW, Yago T, McEver RP, Zhu C (2003) Direct observation of catch bonds involving cell-adhesion molecules. Nature 423:190–193

Marszalek PE, Lu H, Li H, Carrion-Vazquez M, Oberhauser AF, Schulten K, Fernandez JM (1999) Mechanical unfolding intermediates in titin modules. Nature 402:100–103

Matin TR, Sigdel KP, Utjesanovic M, Marsh BP, Gallazzi F, Smith VF, Kosztin I, King GM (2017) Single-molecule peptide-lipid affinity assay reveals interplay between solution structure and partitioning. Langmuir 33:4057–4065

Matin TR, Utjesanovic M, Sigdel KP, Smith VF, Kosztin I, King GM (2020) Characterizing the locus of a peripheral membrane protein–lipid bilayer interaction underlying protein export activity in *E. coli*. Langmuir 36:2143–2152

Merkel R, Nassoy P, Leung A, Ritchie K, Evans E (1999) Energy landscapes of receptor-ligand bonds explored with dynamic force spectroscopy. Nature 397:50–53

Min D, Jefferson RE, Bowie JU, Yoon TY (2015) Mapping the energy landscape for second-stage folding of a single membrane protein. Nat Chem Biol 11:981–987

Mori T, Miyashita N, Im W, Feig M, Sugita Y (2016) Molecular dynamics simulations of biological membranes and membrane proteins using enhanced conformational sampling algorithms. Biochem Biophys Acta 1858:1635–1651

Oesterhelt F, Oesterhelt D, Pfeiffer M, Engel A, Gaub HE, Muller DJ (2000) Unfolding pathways of individual bacteriorhodopsins. Science 288:143–146

Onuchic JN, Luthey-Schulten Z, Wolynes PG (1997) Theory of protein folding: the energy landscape perspective. Annu Rev Phys Chem 48:545–600

Perkins TT (2009) Optical traps for single molecule biophysics: a primer. Laser Photonics Rev 3:203–220

Phillips R, Ursell T, Wiggins P, Sens P (2009) Emerging roles for lipids in shaping membrane-protein function. Nature 459:379–385

Pogorelov TV, Vermaas JV, Arcario MJ, Tajkhorshid E (2014) Partitioning of amino acids into a model membrane: capturing the interface. J Phys Chem B 118:1481–1492

Posokhov YO, Gottlieb PA, Morales MJ, Sachs F, Ladokhin AS (2007) Is lipid bilayer binding a common property of inhibitor cysteine knot ion-channel blockers? Biophys J 93:L20–L22

Reshetnyak YK, Segala M, Andreev OA, Engelman DM (2007) A monomeric membrane peptide that lives in three worlds: in solution, attached to, and inserted across lipid bilayers. Biophys J 93:2363–2372

Rief M, Gautel M, Oesterhelt F, Fernandez JM, Gaub HE (1997) Reversible unfolding of individual titin immunoglobulin domains by AFM. Science 276:1109–1112

Roussel G, White SH (2020) The SecA ATPase motor protein binds to *Escherichia coli* liposomes only as monomers. Biochim Biophys Acta Biomembr 1862:183358

Sackmann E (1996) Supported membranes: scientific and practical applications. Science 271:43–48

Sanganna Gari RR, Chattrakun K, Marsh BP, Mao C, Chada N, Randall LL, King GM (2019) Direct visualization of the *E. coli* Sec translocase engaging precursor proteins in lipid bilayers. Sci Adv 5:eaav9404

Schlierf M, Li H, Fernandez JM (2004) The unfolding kinetics of ubiquitin captured with single-molecule force-clamp techniques. Proc Natl Acad Sci USA 101:7299–7304

Schlierf M, Rief M (2006) Single-molecule unfolding force distributions reveal a funnel-shaped energy landscape. Biophys J 90:L33-35

Schwierz N, Krysiak S, Hugel T, Zacharias M (2016) Mechanism of reversible peptide-bilayer attachment: combined simulation and experimental single-molecule study. Langmuir ACS J Surf Colloids 32:810–821

Serdiuk T, Balasubramaniam D, Sugihara J, Mari SA, Kaback HR, Muller DJ (2016) YidC assists the stepwise and stochastic folding of membrane proteins. Nat Chem Biol 12:911–917

Shibata M, Yamashita H, Uchihashi T, Kandori H, Ando T (2010) High-speed atomic force microscopy shows dynamic molecular processes in photoactivated bacteriorhodopsin. Nat Nanotechnol 5:208–212

Stetter FW, Cwiklik L, Jungwirth P, Hugel T (2014) Single lipid extraction: the anchoring strength of cholesterol in liquid-ordered and liquid-disordered phases. Biophys J 107:1167–1175

Ulmschneider JP, Smith JC, White SH, Ulmschneider MB (2011) In silico partitioning and transmembrane insertion of hydrophobic peptides under equilibrium conditions. J Am Chem Soc 133:15487–15495

Utjesanovic M, Matin TR, Sigdel KP, King GM, Kosztin I (2019) Multiple stochastic pathways in forced peptide–lipid membrane detachment. Sci Rep 9:451

Vasquez-Montes V, Gerhart J, King KE, Thevenin D, Ladokhin AS (2018) Comparison of lipid-dependent bilayer insertion of pHLIP and its P20G variant. Bba Biomembranes 1860:534–543

Walder R, Van Patten WJ, Ritchie DB, Montange RK, Miller TW, Woodside MT, Perkins TT (2018) High-precision single-molecule characterization of the folding of an HIV RNA hairpin by atomic force microscopy. Nano Lett 18:6318–6325

Wang Y, Zhao T, Wei D, Strandberg E, Ulrich AS, Ulmschneider JP (2014) How reliable are molecular dynamics simulations of membrane active antimicrobial peptides? Biochim Biophys Acta 1838:2280–2288

White SH, Ladokhin AS, Jayasinghe S, Hristova K (2001) How membranes shape protein structure. J Biol Chem 276:32395–32398

White SH, Wimley WC (1999) Membrane protein folding and stability: physical principles. Annu Rev Biophys Biomol Struct 28:319–365

Wieland JA, Gewirth AA, Leckband DE (2005) Single-molecule measurements of the impact of lipid phase behavior on anchor strengths. J Phys Chem B 109:5985–5993

Wiener MC, White SH (1992) Structure of a fluid dioleoylphosphatidylcholine bilayer determined by joint refinement of X-ray and neutron-diffraction data. 3 Complete structure. Biophys J 61:434–447

Wimley WC, White SH (1996) Experimentally determined hydrophobicity scale for proteins at membrane interfaces. Nat Struct Biol 3:842–848

Woodside MT, Block SM (2014) Reconstructing folding energy landscapes by single-molecule force spectroscopy. Annu Rev Biophys 43:19–39

Yu H, Siewny MG, Edwards DT, Sanders AW, Perkins TT (2017) Hidden dynamics in the unfolding of individual bacteriorhodopsin proteins. Science 355:945–950

Zimmermann JL, Nicolaus T, Neuert G, Blank K (2010) Thiol-based, site-specific and covalent immobilization of biomolecules for single-molecule experiments. Nat Protoc 5:975–985

Zocher M, Roos C, Wegmann S, Bosshart PD, Dotsch V, Bernhard F, Muller DJ (2012) Single-molecule force spectroscopy from nanodiscs: an assay to quantify folding, stability, and interactions of native membrane proteins. ACS Nano 6:961–971